

# The dynamics of starvation and recovery

2 Justin D. Yeakel \* † ‡ §, Christopher P. Kempes † ‡, and Sidney Redner † ¶ ‡

3 \*School of Natural Science, University of California Merced, Merced, CA, †The Santa Fe Institute, Santa Fe, NM, ¶Department of Physics, Boston University, Boston  
4 MA, ‡Contributed equally, and §To whom correspondence should be addressed: jdyeakel@gmail.com

5 Submitted to Proceedings of the National Academy of Sciences of the United States of America

6 The eco-evolutionary dynamics of species is fundamentally linked  
7 to the energetic constraints of its constituent individuals. Of par-  
8 ticular importance are the tradeoffs between reproduction and  
9 the dynamics of starvation and recovery in resource-limited envi-  
10 ronments. To elucidate the consequences of this tradeoff, we  
11 introduce a minimal nutritional state-structured model that in-  
12 corporates two classes of consumer: nutritionally replete con-  
13 sumers that reproduce, and undernourished, non-reproducing  
14 consumers that are susceptible to mortality. As a function of the  
15 transition rates between these replete and undernourished states  
16 that are determined by the presence or absence of resources,  
17 the consumer populations can either undergo cyclic dynamics or  
18 reach a steady state. We obtain strong constraints on starvation  
19 and recovery rates by deriving allometric scaling relationships  
20 and find that population dynamics subject to these constraints  
21 can approach the cyclic regime but are typically driven to a steady  
22 state. Moreover, we find that these rates fall within a ‘refuge’ in pa-  
23 rameter space, where the probability of extinction of the consumer  
24 population is minimized. Thus we identify a potential mechanism  
25 that may both drive and constrain the dynamics of animal pop-  
26ulations. Our model provides a natural framework that predicts  
27 maximum body size for mammals by determining the relative sta-  
28 bility of an otherwise homogeneous population to a mutant pop-  
29 ulation with altered percent body fat. For body masses  $\lesssim 10^7$  g,  
30 individuals with increased energetic reserves can invade resident  
31 populations, and vice versa for body mass  $\gtrsim 10^7$  g, thus providing  
32 a principled mechanism for a within-lineage driver of Cope’s rule.

33 foraging | starvation | reproduction

34 **Significance Statement** Energetic investment in somatic mainte-  
35 nance and growth vs. reproduction directly impacts the dynamics of  
36 populations among species. Here, we construct a Nutritional State-  
37 structured Model (NSM) to assess the population-level effects of star-  
38 vation and recovery of a consumer population in a resource-limited en-  
39 vironment, and use allometric scaling relationships for mammals to es-  
40 tablish all timescales and rates. Our model reveals that mammalian  
41 energetic rates minimize the probability of stochastic extinction, estab-  
42 lishes dynamic bounds on mammalian body size while providing inde-  
43 pendent theoretical support for the energy equivalence hypothesis, and  
44 provides a mechanistic driver for the evolutionary trend towards larger  
45 body size known as Cope’s rule.

## 46 Introduction

47 The behavioral ecology of all organisms is influenced by the en-  
48 ergetic state of individuals, which directly influences how they  
49 invest reserves in uncertain environments. Such behaviors are  
50 generally manifested as tradeoffs between investing in somatic  
51 maintenance and growth, or allocating energy towards repro-  
52 duction [1, 2, 3]. The timing of these behaviors responds to  
53 selective pressure, as the choice of the investment impacts fu-  
54 ture fitness [4, 5, 6]. The influence of resource limitation on an  
55 organism’s ability to maintain its nutritional stores may lead to  
56 repeated delays or shifts in reproduction over the course of an  
57 organism’s life.

58 The balance between (a) somatic growth and maintenance,  
59 and (b) reproduction depends on resource availability [7]. For  
60 example, reindeer invest less in calves born after harsh win-  
61 ters (when the mother’s energetic state is depleted) than in  
62 calves born after moderate winters [8]. Many bird species in-  
63 vest differently in broods during periods of resource scarcity

64 compared to normal periods [9, 10], sometimes delaying or even  
65 foregoing reproduction for a breeding season [1, 11, 12]. Even  
66 freshwater and marine zooplankton have been observed to avoid  
67 reproduction under nutritional stress [13], and those that do  
68 reproduce have lower survival rates [2]. Organisms may also  
69 separate maintenance and growth from reproduction over space  
70 and time: many salmonids, birds, and some mammals return to  
71 migratory breeding grounds to reproduce after one or multiple  
72 seasons in resource-rich environments where they accumulate  
73 nutritional reserves [14, 15, 16].

74 Physiology also plays an important role in regulating re-  
75 productive expenditures during periods of resource limitation.  
76 The data collected thus far has shown that diverse mammals (47  
77 species in 10 families) exhibit delayed implantation, whereby fe-  
78 males postpone fetal development (blastocyst implantation) un-  
79 til nutritional reserves can be accumulated [17, 18]. Many other  
80 many species (including humans) suffer irregular menstrual cy-  
81 cling and higher abortion rates during periods of nutritional  
82 stress [19, 20]. In the extreme case of unicellular organisms,  
83 nutrition is unavoidably linked to reproduction because the nu-  
84 tritional state of the cell regulates all aspects of the cell cycle  
85 [21]. The existence of so many independently evolved mech-  
86 anisms across such a diverse suite of organisms highlights the im-  
87 portance and universality of the fundamental tradeoff between  
88 somatic and reproductive investment. However the general dy-  
89 namic implications of these constraints are unknown.

90 Though straightforward conceptually, incorporating the en-  
91 ergic dynamics of individuals [22] into a population-level  
92 framework [22, 23] presents numerous mathematical obsta-  
93 cles [24]. An alternative approach involves modeling the  
94 macroscale relations that guide somatic versus reproductive  
95 investment in a consumer-resource system. For example,  
96 macroscale Lotka-Volterra models assume that the growth rate  
97 of the consumer population depends on resource density, thus  
98 implicitly incorporating the requirement of resource availability  
99 for reproduction [25].

100 In this work, we adopt an alternative approach in which we  
101 explicitly account for resource limitation and the subsequent  
102 effects of starvation. Namely, only individuals with sufficient  
103 energetic reserves can reproduce. Such a constraint leads to  
104 reproductive time lags due to some members of the population  
105 going hungry and then recovering. Additionally, we incorporate  
106 the idea that reproduction is strongly constrained allometrically  
107 [3], and is not generally linearly related to resource density. As  
108 we shall show, these constraints influence the ensuing popula-

## Reserved for Publication Footnotes

109 tion dynamics in dramatic ways.

110

### 111 Nutritional state-structured model (NSM)

112 We begin by defining a minimal Nutritional State-structured  
113 population Model (NSM), where the consumer population is  
114 partitioned into two states: (a) an energetically replete (full)  
115 state  $F$ , where the consumer reproduces at a constant rate  $\lambda$   
116 and does not die from starvation, and (b) an energetically de-  
117 ficient (hungry) state  $H$ , where the consumer does not repro-  
118 duce but dies by starvation at rate  $\mu$ . The underlying resource  
119  $R$  evolves by logistic growth with an intrinsic growth rate  $\alpha$   
120 and a carrying capacity equal to one. Consumers transition  
121 from the full state  $F$  to the hungry state  $H$  at a rate  $\sigma$ —the  
122 starvation rate—and also in proportion to the absence of re-  
123 sources ( $1 - R$ ). Conversely, consumers recover from state  $H$   
124 to state  $F$  at rate  $\rho$  and in proportion to  $R$ . Resources are  
125 also eaten by the consumers—at rate  $\rho$  by hungry consumers  
126 and at rate  $\beta < \rho$  by full consumers. This inequality accounts  
127 for hungry consumers requiring more resources to replace lost  
128 body tissue. The NSM represents a fundamental extension of  
129 the idealized starving random walk model of foraging, which  
130 focuses on resource depletion, to include reproduction and re-  
131 source replenishment [26, 27, 28].

In the mean-field approximation, in which the consumers  
and resources are perfectly mixed, their densities evolve accord-  
ing to the rate equations

$$\begin{aligned}\dot{F} &= \lambda F + \rho \frac{c}{k} RH - \sigma(1 - R) F, \\ \dot{H} &= \sigma(1 - R) F - \rho \frac{c}{k} RH - \mu H, \\ \dot{R} &= \alpha R(1 - R) - (\rho R + \delta) H - \beta F\end{aligned}$$

This system of nondimensional equations follows from a set  
of first-principle relationships for resource consumption and  
growth, where  $c/k$  scales the somatic regeneration of body tissue  
sue from resources and is  $\approx 2$  (please see the supplement for a  
full derivation and the dimensional form). Notice that the total  
consumer density  $F+H$  evolves according to  $\dot{F}+\dot{H} = \lambda F - \mu H$ .  
This resembles the equation of motion for the predator density  
in the classic Lotka-Volterra model [29], except that the  
resource density does not appear in the growth term. As dis-  
cussed above, the attributes of reproduction and mortality have  
been explicitly apportioned to the full and hungry consumers,  
respectively, so that the growth in the total density is decoupled  
from the resource density.

Equation [1] has three fixed points: two trivial fixed points  
at  $(F^*, H^*, R^*) = (0, 0, 0)$  and  $(0, 0, 1)$ , and one non-trivial,  
internal fixed point at

$$\begin{aligned}F^* &= \frac{(\sigma - \lambda)\alpha\lambda k\mu^2(c\rho + k\mu)}{A(\lambda\rho B + k\mu\sigma[\beta\mu + \lambda(\delta + \rho)])}, \\ H^* &= \frac{(\sigma - \lambda)\alpha\lambda^2 k\mu(c\rho + k\mu)}{A(\lambda\rho B + k\mu\sigma[\beta\mu + \lambda(\delta + \rho)])}, \\ R^* &= (\sigma - \lambda)k\mu/A.\end{aligned}$$

where  $A = (c\rho + k\mu\sigma)$  and  $B = (c\beta\mu + c\lambda\delta - k\lambda\mu)$ . The stability of this fixed point is determined by the Jacobian matrix  $\mathbf{J}$ , where each matrix element  $J_{ij} = \partial\dot{X}_i/\partial X_j$  when evaluated at the internal fixed point, and  $\mathbf{X}$  is the vector  $(F, H, R)$ . The parameters in Eq. [1] are such that the real part of the largest eigenvalue of  $\mathbf{J}$  is negative, so that the system is stable with respect to small perturbations from the fixed point. Because this fixed point is unique, it is the global attractor for all population trajectories for any initial condition where the resource and consumer densities are both nonzero.

From Eq. [2], an obvious constraint on the NSM is that the reproduction rate  $\lambda$  must be less than the starvation rate

$\sigma$ , so that  $R^*$  is positive. In fact, when the resource density  $R = 0$ , the rate equation for  $F$  gives exponential growth of  $F$  for  $\lambda > \sigma$ . The condition  $\sigma = \lambda$  represents a transcritical (TC) bifurcation [30] that demarcates the physical regime from the unphysical regime where  $F$  would grow exponentially with time. The biological implication of the constraint  $\lambda < \sigma$  has a simple interpretation—the rate at which a macroscopic organism loses mass due to lack of resources is generally much faster than the rate of reproduction. As we will discuss below, this inequality is a natural consequence of allometric constraints [3]

$R$  evolves by logistic growth with an intrinsic growth rate  $\alpha$  for organisms within empirically observed body size ranges.

In the physical regime of  $\lambda < \sigma$ , the fixed point [2] may either be a stable node or a limit cycle (Fig. 1). In continuous-time systems, a limit cycle arises when a pair of complex conjugate eigenvalues crosses the imaginary axis to attain positive real parts [31]. This Hopf bifurcation is defined by  $\text{Det}(\mathbf{S}) = 0$ , also eaten by the consumers—at rate  $\rho$  by hungry consumers with  $\mathbf{S}$  the Sylvester matrix, which is composed of the coefficients of the characteristic polynomial of the Jacobian matrix [32]. As the system parameters are tuned to be within the stable regime but close to the Hopf bifurcation, the amplitude of the transient but decaying cycles become large. Given that ecological systems are constantly being perturbed [33], the onset of transient cycles, even though they decay with time in the mean-field description, can increase the extinction risk [34, 35, 36]. Thus the distance of a system from the Hopf bifurcation provides a measure of its persistence.

When the starvation rate  $\sigma \gg \lambda$ , a substantial fraction of the consumers are driven to the hungry non-reproducing state. Because reproduction is inhibited, there is a low steady-state consumer density and a high steady-state resource density. However, if  $\sigma/\lambda \rightarrow 1$  from above, the population is overloaded with energetically-replete (reproducing) individuals, thereby promoting oscillations between the consumer and resource densities (Fig. 1).

Whereas the relation between consumer growth rate  $\lambda$  and the starvation rate  $\sigma$  defines an absolute bound of biological feasibility—the TC bifurcation— $\sigma$  also determines the sensitivity of the consumer population to changes in resource density. When  $\sigma \gg \lambda$ , the steady-state population density is small, thereby increasing the risk of stochastic extinction. On the other hand, as  $\sigma$  decreases, the system will ultimately be poised either near the TC or the Hopf bifurcation (Fig. 1). If the recovery rate  $\rho$  is sufficiently small, the TC bifurcation is reached and the resource eventually is eliminated. If  $\rho$  exceeds a threshold value, cyclic dynamics will develop as the Hopf bifurcation is approached.

#### 204 Role of allometry

While there are no a priori constraints on the parameters in the NSM, most organisms correspond to restricted portions of the parameter space. Here we use allometric scaling relations to constrain the covariation of rates in a principled and biologically meaningful manner. Allometric scaling relations highlight common constraints and average trends across large ranges in body size and species diversity. Many of these relations can be

derived from a small set of assumptions and below we describe a framework to determine the covariation of timescales and rates across the range of mammals for each of the key parameters of our model (cf. [37]). We are thereby able to define the regime of dynamics occupied by the entire class of mammals along with the key differences between the largest and smallest mammals.

Nearly all of the rates described in the NSM are determined by consumer metabolism, which can be used to describe a variety of organismal features [38]. The scaling relation between an organism's metabolic rate  $B$  and its body mass  $M$  at reproductive maturity is known to scale as  $B = B_0 M^\eta$  [39], where the scaling exponent  $\eta$  is typically close to 2/3 or 3/4 for metazoans

(e.g., [38]), and has taxonomic shifts for unicellular species between  $\eta \approx 1$  in eukaryotes and  $\eta \approx 1.76$  in bacteria [40, 3]. An organism's metabolic rate  $B$  is proportional to the cost of tissue maintenance in the absence of growth (i.e., when the body mass is  $M$ ). By definition  $B = \beta/\xi$ , where  $\beta$  is the rate at which resources are consumed for full consumers (see Eq. [1]) and where  $\xi$  is related to the conversion efficiency of resource to consumer tissue (Supporting Information).

Several efforts have shown how a partitioning of  $B$  between growth and maintenance purposes can be used to derive a general equation for both the growth trajectories and growth rates of organisms ranging from bacteria to metazoans [41, 42, 43, 44, 3]. This relation is derived from the simple balance condition [41, 42, 43, 44, 3]

$$B_0 m^\eta = E_m \dot{m} + B_m m,$$

[3]

$$\dot{m}E'_m = -B_m m$$

[7]

where  $E_m$  is the energy needed to synthesize a unit of mass,  $B_m$  is the metabolic rate to support an existing unit of mass, and  $m$  is the mass of the organism at any point in its development. This balance has the general solution [45, 3]

$$\left(\frac{m(t)}{M}\right)^{1-\eta} = 1 - \left[1 - \left(\frac{m_0}{M}\right)^{1-\eta}\right] e^{-a(1-\eta)t/M^{1-\eta}}$$

[4]

where, for  $\eta < 1$ ,  $M = (B_0/B_m)^{1/(1-\eta)}$  is the asymptotic mass,  $a = B_0/E_m$ , and  $m_0$  is mass at birth. We now use this solution to define the timescale of reproduction and recovery from starvation (Fig. 2; see [42] for a detailed presentation of these timescales). The time that it takes to reach a particular mass  $\epsilon M$  is given by the timescale

$$\tau(\epsilon) = \ln \left[ \frac{1 - (m_0/M)^{1-\eta}}{1 - \epsilon^{1-\eta}} \right] \frac{M^{1-\eta}}{a(1-\eta)}$$

[5]

where we will define values of  $\epsilon$  to describe a set of rates within our model. For the time to reproduce,  $t_\lambda = \tau(\epsilon_\lambda)$ , where  $\epsilon_\lambda$  is the fraction of the asymptotic mass where an organism is reproductively mature and should be close to one (typically  $\epsilon_\lambda \approx 0.95$  [41]). The growth rate is then given by  $\lambda = \ln(v)/t_\lambda$  where  $v$  is the number of offspring produced, and for any constant value of  $\epsilon_\lambda$  this will scale like  $\lambda \propto M^{\eta-1}$  for  $M \gg m_0$  [41, 42, 43, 44, 3].

The rate of recovery  $\rho = 1/t_\rho$  requires that an organism accrues sufficient tissue to transition from the hungry to the full state. Since only certain tissues can be digested for energy (for example the brain cannot be degraded to fuel metabolism), we define the rates for starvation, death, and recovery by the timescales required to reach, or return from, specific fractions of the replete-state mass (Fig. 3; see Supporting Information, Table I for parameterizations). We define  $m_\sigma = \epsilon_\sigma M$ , where  $\epsilon_\sigma < 1$  is the fraction of replete-state mass where reproduction ceases. This fraction will be modified if tissue composition systematically scales with adult mass. For example, making use of the observation that body fat in mammals scales with overall body size according to  $M_{\text{fat}} = f_0 M^\gamma$  and assuming that once this mass is fully digested the organism starves, this would imply that  $\epsilon_\sigma = 1 - f_0 M^\gamma/M$ . It follows that the recovery timescale,  $t_\rho$ , is the time to go from  $m = \epsilon_\sigma \epsilon_\lambda M$  to  $m = \epsilon_\lambda M$  (Fig. 2). Using Eqs. [4] and [5] this timescale is given by simply considering an adjusted starting mass of  $m'_0 = \epsilon_\sigma \epsilon_\lambda M$ , in which case

$$t_\rho = \ln \left[ \frac{1 - (\epsilon_\sigma \epsilon_\lambda)^{1-\eta}}{1 - \epsilon^{1-\eta}} \right] \frac{M^{1-\eta}}{a'(1-\eta)}$$

[6]

where  $a' = B_0/E'_m$  accounts for possible deviations in the biosynthetic energetics during recovery (see Supporting Information). It should be noted that more complicated ontogenetic

models explicitly handle storage [44], whereas this feature is implicitly covered by the body fat scaling in our framework. To determine the starvation rate,  $\sigma$ , we are interested in the time required for an organism to go from a mature adult that reproduces at rate  $\lambda$ , to a reduced-mass hungry state where production is impossible. For starving individuals we assume that an organism must meet its maintenance requirements using the digestion of existing mass as the sole energy source. This assumption implies the following simple metabolic balance

$$\dot{m} = -\frac{a'}{M^{1-\eta}} m$$

[8]

[3]

where  $E'_m$  is the amount of energy stored in a unit of existing body mass which differs from  $E_m$ , the energy required to synthesize a unit of biomass [44]. Given the replete mass,  $M$ , of an organism, the above energy balance prescribes the mass trajectory of a non-consuming organism:

$$m(t) = M e^{-a't/M^{1-\eta}}.$$

[9]

The time scale for starvation is given by the time it takes  $m(t)$  to reach  $\epsilon_\sigma M$ , which gives

$$t_\sigma = -\frac{M^{1-\eta}}{a'} \ln(\epsilon_\sigma).$$

[10]

The starvation rate is then  $\sigma = 1/t_\sigma$ , which scales with replete-state mass as  $1/M^{1-\eta} \ln(1 - f_0 M^\gamma/M)$ . An important feature is that  $\sigma$  does not have a simple scaling dependence on  $\lambda$  (Fig. 3), which is important for the dynamics that we later discuss.

The time to death should follow a similar relation, but defined by a lower fraction of replete-state mass,  $m_\mu = \epsilon_\mu M$ . Suppose, for example, that an organism dies once it has digested all fat and muscle tissues, and that muscle tissue scales with body mass according to  $M_{\text{musc}} = u_0 M^\zeta$ . This gives  $\epsilon_\mu = 1 - (f_0 M^\gamma + u_0 M^\zeta)/M$ . Muscle mass has been shown to be roughly proportional to body mass [46] in mammals and thus  $\epsilon_\mu$  is merely  $\epsilon_\sigma$  minus a constant. The time to death is the total time to reach  $\epsilon_\mu M$  minus the time to starve, or

$$t_\mu = -\frac{M^{1-\eta}}{a'} \ln(\epsilon_\mu) - t_\sigma,$$

[11]

and  $\mu = 1/t_\mu$ .

Although the rate equations [1] are general, here we focus on parameterizations for terrestrial-bound endotherms, specifically mammals, which range from a minimum of  $M \approx 1\text{g}$  (the Etruscan shrew *Suncus etruscus*) to a maximum of  $M \approx 10^7\text{g}$  (the late Eocene to early Miocene Indricotheriinae). Investigating other classes of organisms would simply involve altering the metabolic exponents and scalings associate with  $\epsilon$ . Moreover, we emphasize that our allometric equations describe mean relationships, and do not account for the (sometimes considerable) variance associated with individual species.

### Stabilizing effects of allometric constraints

As the allometric derivations of the NSM rate laws reveal, starvation and recovery rates are not independent parameters, and the biologically relevant portion of the phase space shown in Fig. 1 is constrained via covarying parameters. Given the parameters of terrestrial endotherms, we find that the starvation rate  $\sigma$  and the recovery rate  $\rho$  are constrained to lie within a small window of potential values (Fig. 4) for the known range of body sizes  $M$ . We thus find that the dynamics for all mammalian body sizes is confined to the steady-state regime of the NSM and that limit-cycle behavior is precluded. Moreover, for

330 larger  $M$ , the distance to the Hopf bifurcation increases, while 395 allometrically-determined parameters fall within this low ex-  
331 uncertainty in allometric parameters (20% variation around the 396 extinction probability region suggests that the NSM dynamics  
332 mean; Fig. 4) results in little qualitative difference in the dis- 397 may both drive—and constrain—natural animal populations.  
333 tance to the the Hopf bifurcation. These results suggest that 398

334 small mammals are more prone to population oscillations—both 399 **Dynamic and energetic barriers to body size**  
335 stable limit cycles and transient cycles—than mammals with 400 Metabolite transport constraints are widely thought to place  
336 larger body size. Thus our NSM model predicts that popula- 401 strict boundaries on biological scaling [54, 55, 38] and thereby  
337 tion cycles should be less common for larger species and more 402 lead to specific predictions on the minimum possible body size  
338 common for smaller species, particularly in environments where 403 for organisms [56]. Above this bound, a number of energetic and  
339 resources are limiting. 404 evolutionary mechanisms have been explored to assess the costs  
340 It should be noted that previous studies have used allomet- 405 and benefits associated with larger body masses, particularly  
341 ric constraints to explain the periodicity of cyclic populations 406 for mammals. One important such example is the *fasting en-*  
342 [47, 48, 49], suggesting a period  $\propto M^{0.25}$ . However this relation 407 *durance hypothesis*, which contends that larger body size, with  
343 seems to hold only for some species [50], and potential drivers 408 consequent lower metabolic rates and increased ability to main-  
344 range from predator and/or prey lifespans to competitive dy- 409 tain more endogenous energetic reserves, may buffer organisms  
345 namics [51, 52]. Statistically significant support for the exis- 410 against environmental fluctuations in resource availability [57].  
346 tence of population cycles among mammals is predominantly 411 Over evolutionary time, terrestrial mammalian lineages show a  
347 based on time series for small mammals [53], in agreement with 412 significant trend towards larger body size (known as Cope's  
348 our predictions of more pronounced transient dynamics, given 413 rule) [58, 59, 60, 61], and it is thought that within-lineage  
349 how close these points are to the Hopf bifurcation. On the other 414 drivers generate selection towards an optimal upper bound of  
350 hand, the longer gestational times and the increased difficulty 415 roughly  $10^7$  grams [58], a value that is likely limited by higher  
351 in measurements, precludes obtaining similar-quality data for 416 extinction risk for large taxa over longer timescales [59]. These  
352 larger organisms. 417 trends are thought to be driven by a combination of climate  
353 **Extinction risk** 418 change and niche availability [61]; however the underpinning  
354 Within our model, higher rates of starvation result in a larger 419 energetic costs and benefits of larger body sizes, and how they  
355 flux of the population to the hungry state. In this state re- 420 influence dynamics over ecological timescales, have not been ex-  
356 production is absent, thus increasing the likelihood of extinc- 421 plored. We argue that the NSM provides a suitable framework  
357 tion. From the perspective of population survival, it is the rate 422 to explore these issues.

358 of starvation relative to the rate of recovery that determines 423 The NSM correctly predicts that species with smaller  
359 the long-term dynamics of the various species (Fig. 1). We 424 masses have larger steady-state population densities (Fig. 6A).  
360 therefore examine the competing effects of cyclic dynamics vs. 425 Moreover, we show that the NSM provides independent theo-  
361 changes in steady state density on extinction risk as a function 426 retical support for the energy equivalence hypothesis [62, 63].  
362 of  $\sigma$  and  $\rho$ . To this end, we computed the probability of ex- 427 The energy equivalence hypothesis argues that the total energy  
363 tinction, where we define extinction as a population trajectory 428 use,  $B_{tot}$ , of a population is constant independent of species size  
364 falling below one fifth of the allometrically constrained steady 429 (e.g. [62, 63]). This hypothesis is based on observations show-  
365 state at any time between  $t = 10^5$  and  $t \leq 10^8$ . This procedure 430 ing that the abundance,  $N$ , of a species is proportional to the  
366 is repeated for 1000 replicates of the continuous-time system 431 inverse of individual metabolism (e.g.  $N \propto M^{-3/4}/B_0$ ) (e.g.  
367 shown in Eq. 1 for an organism of  $M = 100$  grams. In each 432 [62, 63]). This is usually stated as  $B_{tot} = NB = C$  where  $C$   
368 replicate the initial densities are chosen to be  $X(F^*, H^*, R^*)$ , 433 is a constant, and has been shown to hold in both mammalian  
369 with  $X$  a random variable that is uniformly distributed in  $[0, 2]$ . 434 and vascular plant communities [62, 63]. Figure 6A shows that  
370 By allowing the rate of starvation to vary, we assessed extinc- 435 both  $F^*$  and  $H^*$  scale like  $M^{-\eta}$  over a wide range of organ-  
371 tion risk across a range of values for  $\sigma$  and  $\rho$  between ca.  $10^{-7}$  436 ism sizes and Figure 6B shows that  $F^*B$  is nearly constant  
372 to  $10^{-3}$ . As expected, higher rates of extinction correlate with 437 over this same range. This result if remarkable because it illus-  
373 both high values of  $\sigma$  if  $\rho$  is small, and high values of  $\rho$  if  $\sigma$  is 438 trates that the steady state values of the NSM combined with  
374 small. For low values of  $\sigma$  and high values of  $\rho$ , the increased 439 the derived timescales naturally give rise to the energy equiv-  
375 extinction risk results from transient cycles with larger ampli- 440 alence result. Our model shows that the equivalence breaks  
376 tudes as the system nears the Hopf bifurcation (Fig. 5). For 441 down at the maximum observed body sizes for mammals, sug-  
377 high values of  $\sigma$  and low values of  $\rho$ , higher extinction risk arises 442 gesting that this is a hard limit where deviations outside of this  
378 because of the decrease in the steady state consumer popula- 443 range are energetically suboptimal. A stronger version of this  
379 tion density (Figs. 1B, 5). This interplay creates an ‘extinction 444 statement is that the total metabolic rate of  $F$  and  $H$  becomes  
380 refuge’, such that for a constrained range of  $\sigma$  and  $\rho$ , extinction 445 infinite at a finite mass, occuring at the same scale where the  
381 probabilities are minimized. 446 steady state resources vanish (Fig. 6). This asymptotic behav-  
382 We find that the allometrically constrained values of  $\sigma$  and 447 ior represents an upper bound on mammalian body size and oc-  
383  $\rho$  fall squarely within the extinction refuge (Fig. 5, white point). 448 curs at  $M_{max} = VALUE$ . Moreover,  $M_{max}$ , which is entirely  
384 These values are close enough to the Hopf bifurcation to avoid 449 determined by the population-level consequences of energetic  
385 low steady state densities, and far enough away to avoid large- 450 constraints, is remarkably close to the maximum body size ob-  
386 amplitude transient cycles. The fact that allometric values of  $\sigma$  451 served in the North American mammalian fossil record [58] as  
387 and  $\rho$  fall within this relatively small window supports the possi- 452 well as the mass predicted from an evolutionary model of body  
388 bility that a selective mechanism has constrained the physiolog- 453 size evolution [59].  
389 454 We contend that the NSM provides a mechanistic under-  
390 populations. Such a mechanism would select for organism phys- 455 standing of the energetic dynamics that give rise to both ob-  
391 iology that generates appropriate  $\sigma$  and  $\rho$  values that serve to 456 served limitations on mammalian body size as well as the ob-  
392 minimize extinction risk. This selection could occur via the 457 served trend towards larger body size over evolutionary time.  
393 tuning of body fat percentages, metabolic rates, and biomass 458 The NSM predicts that the steady state resource density  $R^*$   
394 maintenance efficiencies. To summarize, our finding that the 459 decreases with increasing body size of the consumer population  
460 (Fig. 6C), and classic resource competition theory predicts that  
461 the species surviving on the lowest resource abundance will out-

462 compete others [64, 65, 66]. Thus, the combined NSM steady- 494 mal mass to increase if  $M < M_{\text{opt}}$  and decrease if  $M > M_{\text{opt}}$ .  
 463 state dynamics and allometric timescales predict that larger 495 This value is close to but smaller than the asymptotic upper  
 464 mammals have an intrinsic competitive advantage given a com- 496 bound for terrestrial mammal size predicted by the NSM and  
 465 mon resource, but does not offer a within-lineage mechanism by 497 is also remarkable close to independent estimates of the largest  
 466 which larger body sizes are selected for. 498 land mammal [58, 59].

467 To examine whether the NSM could provide such a mecha- 499 While the state of the environment, as well as the compet-  
 468 nism, we begin by noting that a theoretical upper bound on 500 itive landscape, will determine whether specific body sizes are  
 469 mammalian body size is given by  $\epsilon_\sigma = 0$ , where mammals 501 selected for or against [61], we suggest that the dynamics of  
 470 are entirely composed of metabolic reserves, and this occurs 502 starvation and recovery described in the NSM may provide a  
 471 at  $M = 8.3 \times 10^8$ , or  $4.5 \times$  the mass of a blue whale. Next 503 general driving mechanism for the evolution of larger body size  
 472 we examine to what extent a more realistic upper bound to 504 among terrestrial mammals.

473 body mass may serve as an evolutionary attractor, thus provid- 505 The energetics associated with somatic maintenance,  
 474 ing a suitable within-lineage mechanism for Cope's rule. We 506 growth, and reproduction are important elements that influence  
 475 directly assess the susceptibility of an otherwise homogeneous 507 the dynamics of all populations [11]. The NSM is a minimal and  
 476 population to invasion by a mutated subset of the population 508 general model that incorporates the dynamics of starvation and  
 477 (denoted by ') where individuals have a modified proportion 509 recovery that are expected to occur in resource-limited envi-  
 478 of body fat  $M' = M(1 + \chi)$  where  $\chi \in [-1, 1]$ , thus altering 510 ronments. By incorporating allometric relations between the  
 479 the rates of starvation  $\sigma(M')$ , recovery  $\rho(M')$ , and maintenance 511 rates in the NSM, we found: (i) different organismal masses  
 480  $\beta(M')$ . There is no internal fixed point corresponding to a state 512 have distinct population dynamic regimes, (ii) allometrically-  
 481 where both original residents and invaders coexist (except for 513 determined rates of starvation and recovery appear to min-  
 482 the trivial state  $\chi = 0$ ). To assess the susceptibility to invasion 514 imize extinction risk, and (iii) the dynamic consequences of  
 483 as a function of the invader mass, we determine which consumer 515 these rates may introduce additional drivers and hard bound-  
 484 has a lower steady-state resource density for a given value of  $\chi$ . 516 aries on the evolution of minimum and maximum body size.  
 485 We find that for  $1 \leq M < \text{VALUE}_g$ , having additional body 517 We suggest that the NSM offers a means by which the dy-  
 486 fat ( $\chi > 0$ ) results in a higher steady-state invader population 518 namic consequences of energetic constraints can be assessed us-  
 487 density ( $H'^* + F'^* > H^* + F^*$ ). Thus the invader has an in- 519 ing macroscale interactions between and among species. Future  
 488 trinsic advantage over the resident population. However, for 520 efforts will involve exploring the consequences of these dynamics  
 489  $M > \text{VALUE}$ , leaner individuals ( $\chi < 0$ ) have advantageous 521 in a spatially explicit framework, thus incorporating elements  
 490 steady state densities. 522 such as movement costs and spatial heterogeneity, which may  
 491 The observed switch in susceptibility as a function of  $\chi$  at 523 elucidate additional tradeoffs associated with the dynamics of  
 492  $M_{\text{opt}} = \text{VALUE}$  thus serves as an attractor, or an uninvadable 524 starvation and recovery.

493 evolutionary stable state, such that the NSM predicts organi-

498 While the state of the environment, as well as the compet-  
 499 itive landscape, will determine whether specific body sizes are  
 500 selected for or against [61], we suggest that the dynamics of  
 501 starvation and recovery described in the NSM may provide a  
 502 general driving mechanism for the evolution of larger body size  
 503 among terrestrial mammals.

504 The energetics associated with somatic maintenance,  
 505 growth, and reproduction are important elements that influence  
 506 the dynamics of all populations [11]. The NSM is a minimal and  
 507 general model that incorporates the dynamics of starvation and  
 508 recovery that are expected to occur in resource-limited envi-  
 509 ronments. By incorporating allometric relations between the  
 510 rates in the NSM, we found: (i) different organismal masses  
 511 have distinct population dynamic regimes, (ii) allometrically-  
 512 determined rates of starvation and recovery appear to min-  
 513 imize extinction risk, and (iii) the dynamic consequences of  
 514 these rates may introduce additional drivers and hard bound-  
 515 aries on the evolution of minimum and maximum body size.  
 516 We suggest that the NSM offers a means by which the dy-  
 517 namic consequences of energetic constraints can be assessed us-  
 518 ing macroscale interactions between and among species. Future  
 519 efforts will involve exploring the consequences of these dynamics  
 520 in a spatially explicit framework, thus incorporating elements  
 521 such as movement costs and spatial heterogeneity, which may  
 522 elucidate additional tradeoffs associated with the dynamics of  
 523 starvation and recovery.

- 525 1. Martin TE (1987) Food as a Limit on Breeding Birds: A Life-History Perspective. *Annu. Rev. Ecol. Syst.* 18:453–487.
- 526 2. Kirk KL (1997) Life-History Responses to Variable Environments: Starvation and 564 20. Trites AW, Donnelly CP (2003) The decline of Steller sea lions *Eumetopias jubatus*  
565 in Alaska: a review of the nutritional stress hypothesis. *Mammal Review* 33:3–28.
- 527 3. Kempes CP, Dutkiewicz S, Follows MJ (2012) Growth, metabolic partitioning, and 566 21. Glazier DS (2009) Metabolic level and size scaling of rates of respiration and growth  
567 in unicellular organisms. *Funct. Ecol.* 23:963–968.
- 528 4. Mangel M, Clark CW (1988) *Dynamic Modeling in Behavioral Ecology* (Princeton 568 22. Kooijman SALM (2000) *Dynamic Energy and Mass Budgets in Biological Systems*  
569 (Cambridge).
- 529 5. Mangel M (2014) Stochastic dynamic programming illuminates the link between 570 23. Sousa T, Domingos T, Poggiale JC, Kooijman SALM (2010) Dynamic energy budget  
571 theory restores coherence in biology. *Philos. T. Roy. Soc. B* 365:3413–3428.
- 530 6. Yeakel JD, Dominy NJ, Koch PL, Mangel M (2014) Functional morphology, stable 572 24. Diekmann O, Metz JA (2010) How to lift a model for individual behaviour to the  
573 isotopes, and human evolution: a model of consilience. *Evolution* 68:190–203.
- 531 7. Morris DW (1987) Optimal Allocation of Parental Investment. *Oikos* 49:332.
- 532 8. Vrbaas T, Fauchald P, Henaug C, Yoccoz NG (2003) An examination of a com- 574 25. Murdoch WW, Briggs CJ, Nisbet RM (2003) *Consumer-resource Dynamics*, Mono-  
575 graphs in population biology (Princeton University Press).
- 533 9. Daan S, Dijkstra C, Drent R, Meijer T (1988) *Food supply and the annual timing of 576 26. Bénichou O, Redner S (2014) Depletion-Controlled Starvation of a Diffusing Forager.  
577 avian reproduction*.
- 534 10. Jacot A, Valcu M, van Oers K, Kempenaers B (2009) Experimental nest site lim- 578 27. Bénichou O, Chupeau M, Redner S (2016) Role of Depletion on the Dynamics of a  
579 itation affects reproductive strategies and parental investment in a hole-nesting 580 Diffusing Forager.
- 535 11. Stearns SC (1989) Trade-Offs in Life-History Evolution. *Funct. Ecol.* 3:259.
- 536 12. Barboza P, Jorde D (2002) Intermittent fasting during winter and spring affects body 581 28. Chupeau M, Bénichou O, Redner S (2016) Universality classes of foraging with  
582 composition and reproduction of a migratory duck. *J Comp Physiol B* 172:419–434.
- 537 13. Threlkeld ST (1976) Starvation and the size structure of zooplankton communities. 583 29. Murray JD (2011) *Mathematical Biology: I. An Introduction*, Interdisciplinary Applied  
584 Mathematics (Springer New York, Melaka Manipal Medical College (Manipal Campus), International Centre for Health Sciences, Madhav Nagar, Manipal, Udupi District, Karnataka State, India. nayaksathish@yahoo.com) Vol. 110.
- 538 14. Weber TP, Ens BJ, Houston AI (1998) Optimal avian migration: A dynamic model 585 30. Strogatz SH (2008) *Nonlinear Dynamics and Chaos*, With Applications to Physics,  
586 of fuel stores and site use. *Evolutionary Ecology* 12:377–401.
- 539 15. Mduma SAR, Sinclair ARE, Hilborn R (1999) Food regulates the Serengeti wilde- 587 31. Guckenheimer J, Holmes P (1983) *Nonlinear oscillations, dynamical systems, and  
588 beest: a 40-year record. *J. Anim. Ecol.* 68:1101–1122.*
- 540 16. Moore JW, Yeakel JD, Peard D, Lough J, Beere M (2014) Life-history diversity and its 589 32. Gross T, Feudel U (2004) Analytical search for bifurcation surfaces in parameter  
541 importance to population stability and persistence of a migratory fish: steelhead 590 space. *Physica D* 195:292–302.
- 542 17. Mead RA (1989) in *Carnivore Behavior, Ecology, and Evolution* (Springer US, 591 33. Hastings A (2001) Transient dynamics and persistence of ecological systems. *Ecol. Lett.* 4:215–220.
- 543 18. Sandell M (1990) The Evolution of Seasonal Delayed Implantation. *The Quarterly 592 34. Neubert M, Caswell H (1997) Alternatives to resilience for measuring the responses  
544 Review of Biology* 65:23–42.
- 545 19. Bulik CM, et al. (1999) Fertility and Reproduction in Women With Anorexia Nervosa. 593 35. Caswell H, Neubert MG (2005) Reactivity and transient dynamics of discrete-time  
546 *J. Clin. Psychiatry* 60:130–135.
- 547 20. Yodzis P, Innes S (1992) Body Size and Consumer-Resource Dynamics. *Am. Nat.* 594 36. Neubert M, Caswell H (2009) Detecting reactivity. *Ecology*.
- 548 21. Brown J, Gillooly J, Allen A, Savage V, West G (2004) Toward a metabolic theory of 595 37. 600 38. ecology. *Ecology* 85:1771–1789.

- 603 39. West GB, Woodruff WH, Brown JH (2002) Allometric scaling of metabolic rate from 639 molecules and mitochondria to cells and mammals. *Proc. Natl. Acad. Sci. USA* 99: 640  
604 Suppl. 1:2473–2478.

605 40. DeLong JP, Okie JG, Moses ME, Sibly RM, Brown JH (2010) Shifts in metabolic 641 scaling, production, and efficiency across major evolutionary transitions of life. 642 *PNAS* 107:12941–12945.

606 41. West GB, Brown JH, Enquist BJ (2001) A general model for ontogenetic growth. 643 *Nature* 413:628–631.

607 42. Moses ME, et al. (2008) Revisiting a Model of Ontogenetic Growth: Estimating Model 644 Parameters from Theory and Data. <http://dx.doi.org.proxy.lib.sfu.ca/10.1086/679735>

608 43. Gillooly JF, Charnov EL, West GB, Savage VM, Brown JH (2002) Effects of size and 645 temperature on developmental time. *Nature* 417:70–73.

609 44. Hou C, et al. (2008) Energy Uptake and Allocation During Ontogeny. *Science* 646 171:632–645.

610 45. Bettencourt LMA, Lobo J, Helbing D, Kuhnen C, West GB (2007) Growth, innovation, 647 scaling, and the pace of life in cities. *Proc. Natl. Acad. Sci. USA* 104:7301–7306.

611 46. Folland JP, Mc Cauley TM, Williams AG (2008) Allometric scaling of strength mea- 648 surements to body size. *Eur J Appl Physiol* 102:739–745.

612 47. Calder III WA (1983) An allometric approach to population cycles of mammals. *J. 649 Theor. Biol.* 100:275–282.

613 48. Peterson RO, PAGE RE, Dodge KM (1984) Wolves, Moose, and the Allometry of 650 Population Cycles. *Science* 224:1350–1352.

614 49. Krukonis G, Schaffer WM (1991) Population cycles in mammals and birds: Does 651 periodicity scale with body size? *J. Theor. Biol.* 148:469–493.

615 50. Hendriks AJ, Mulder C (2012) Delayed logistic and Rosenzweig(MacArthur models 652 with allometric parameter setting estimate population cycles at lower trophic levels 653 well. *Ecological Complexity* 9:43–54.

616 51. Kendall BE, et al. (1999) Why do populations cycle? A synthesis of statistical and 654 mechanistic modeling approaches. *Ecology* 80:1789–1805.

617 52. Höglstedt G, Seldal T, Breistol A (2005) Period length in cyclic animal populations. 655 *Ecology* 86:373–378.

618 53. Kendall, Prengast, Bjornstad (1998) The macroecology of population dynamics: 656 taxonomic and biogeographic patterns in population cycles. *Ecol. Lett.* 1:160–164.

619 54. Brown J, Marquet P, Taper M (1993) Evolution of body size: consequences of an 657 energetic definition of fitness. *Am. Nat.* 142:573–584.

620 55. West GB, Brown JH, Enquist BJ (1997) A General Model for the Origin of Allometric 658 Scaling Laws in Biology. *Science* 276:122–126.

621 56. West GB, Woodruff WH, Brown JH (2002) Allometric scaling of metabolic rate from 659 molecules and mitochondria to cells and mammals. *Proc. Natl. Acad. Sci. USA* 99:2473–2478.

622 57. Millar J, Hickling G (1990) Fasting Endurance and the Evolution of Mammalian 660 Body Size. *Funct. Ecol.* 4:5–12.

623 58. Alroy J (1998) Cope's rule and the dynamics of body mass evolution in North 661 American fossil mammals. *Science* 280:731.

624 59. Clauset A, Redner S (2009) Evolutionary Model of Species Body Mass Diversification- 662 *Phys. Rev. Lett.* 102:038103.

625 60. Smith F, Boyer A, Brown J, Costa D (2010) The Evolution of Maximum Body Size of 663 Terrestrial Mammals. *Science*.

626 61. Saarinen JJ, et al. (2014) Patterns of maximum body size evolution in Cenozoic 664 land mammals: eco-evolutionary processes and abiotic forcing. *Proc Biol Sci* 281:20132049–20132049.

627 62. Allen AP, Brown JH, Gillooly JF (2002) Global Biodiversity, Biochemical Kinetics, 665 and the Energetic-Equivalence Rule. *Science* 297:1545–1548.

628 63. Enquist BJ, Brown JH, West GB (1998) Allometric scaling of plant energetics and 666 population density : Abstract : Nature. *Nature* 395:163–165.

629 64. Tilman D (1981) Tests of Resource Competition Theory Using Four Species of Lake 667 Michigan Algae. *Ecology* 62:802–815.

630 65. Dutkiewicz S, Follows MJ, Bragg JG (2009) Modeling the coupling of ocean ecology 668 and biogeochemistry. *Global Biogeochem. Cycles* 23:n/a–n/a.

631 66. Barton AD, Dutkiewicz S, Flierl G, Bragg J, Follows MJ (2010) Patterns of Diversity 669 in Marine Phytoplankton. *Science* 327:1509–1511.

**665 ACKNOWLEDGMENTS.** We thank Luis Bettencourt, Jean Philippe Gilbert,  
666 Eric Libby, and Seth Newsome for helpful discussions and comments on the  
667 manuscript. J.D.Y. was supported by startup funds at the University of California,  
668 Merced, and an Omidyar Postdoctoral Fellowship at the Santa Fe Institute. C.P.K.  
669 was supported by an Omidyar Postdoctoral Fellowship at the Santa Fe Institute.  
670 S.R. was supported by grants DMR-1608211 and 1623243 from the National  
671 Science Foundation, and by the John Templeton Foundation, all at the Santa Fe  
672 Institute.

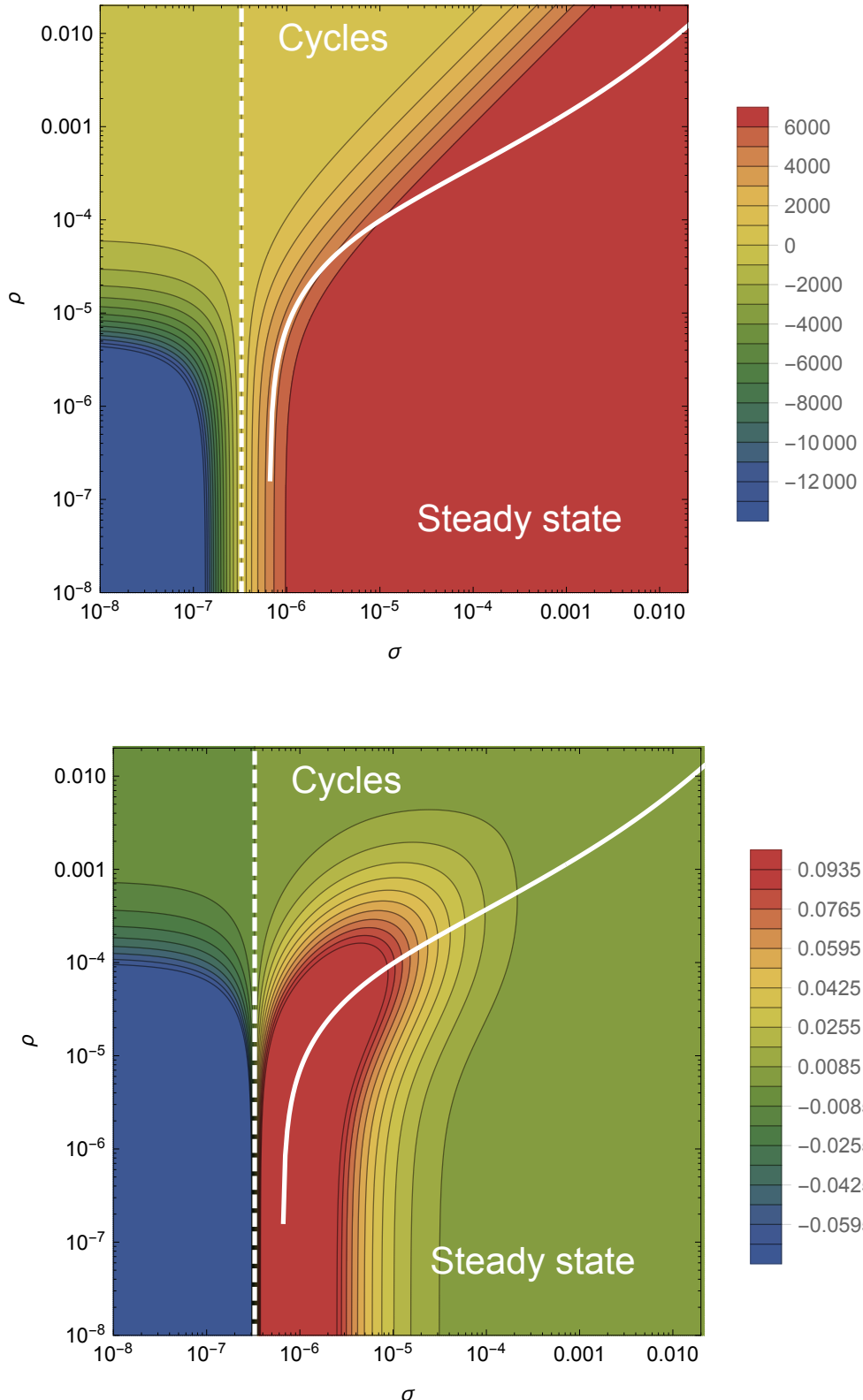


Fig. 1: The transcritical (dashed) and Hopf bifurcation (solid) as a function of the starvation rate  $\sigma$  and recovery rate  $\rho$  for a 100g consumer. These bifurcation conditions separate parameter space into infeasible, cyclic, and steady state dynamic regimes. The color gradient shows the steady state densities for (A) the resource  $R^*$  and the (B) energetically replete consumers  $F^*$ , (warmer colors denote higher densities). Steady state densities for the energetically deficient consumers  $H^*$  (not shown) scale with those for  $F^*$ .

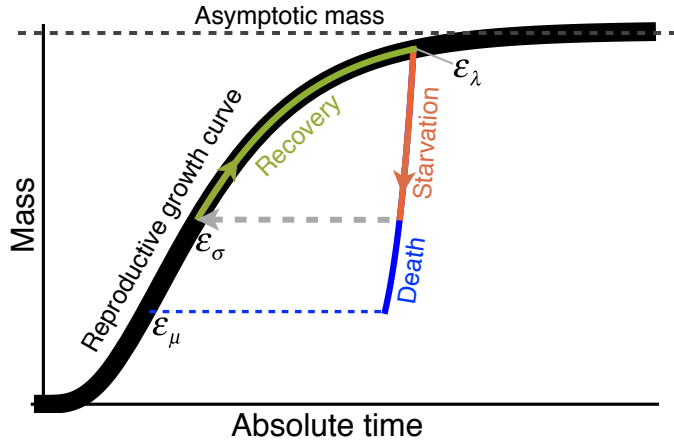


Fig. 2: The growth trajectory over absolute time of an individual organism as a function of body mass. Initial growth follows the black trajectory to an energetically replete reproductive adult mass  $m = \epsilon_\lambda M$  which we assume is 95% asymptotic mass  $M$ . Starvation follows the red trajectory to  $m = \epsilon_\sigma \epsilon_\lambda M$ , and recovery follows the green growth trajectory to the replete adult mass. Alternatively, death from starvation follows the blue trajectory to  $m = \epsilon_\mu \epsilon_\lambda M$ .

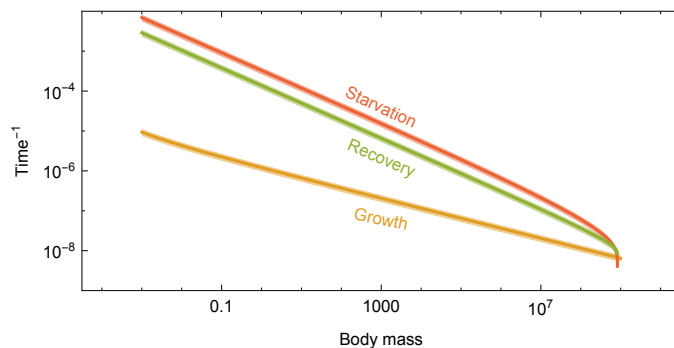


Fig. 3: Allometrically constrained starvation rate  $\sigma$  (red) and recovery rate  $\rho$  (green) relative to the reproductive rate  $\lambda$  (orange) as a function of body mass. The rate of starvation is greater than the rate of reproduction for all realized terrestrial endotherm body sizes. Mean values  $\pm 20\%$  variation are shown by the shaded region for each rate.

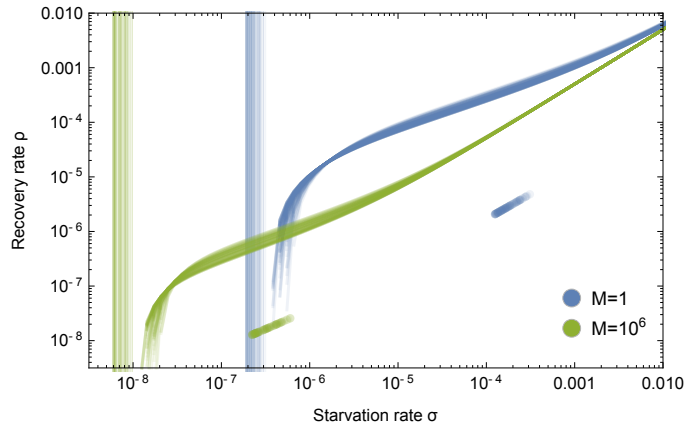


Fig. 4: Transcritical (vertical lines) and Hopf bifurcations (curves) for allometrically determined starvation  $\sigma$  and recovery  $\rho$  rates as a function of different mammalian body sizes:  $M = A \times 10^1\text{g}$  (blue) and  $M = A \times 10^6\text{g}$  (green), where  $A$  is a random uniform variable in  $[1, 9]$ . Points denote realized values of  $\sigma$  and  $\rho$  given the drawn values for  $M$ .

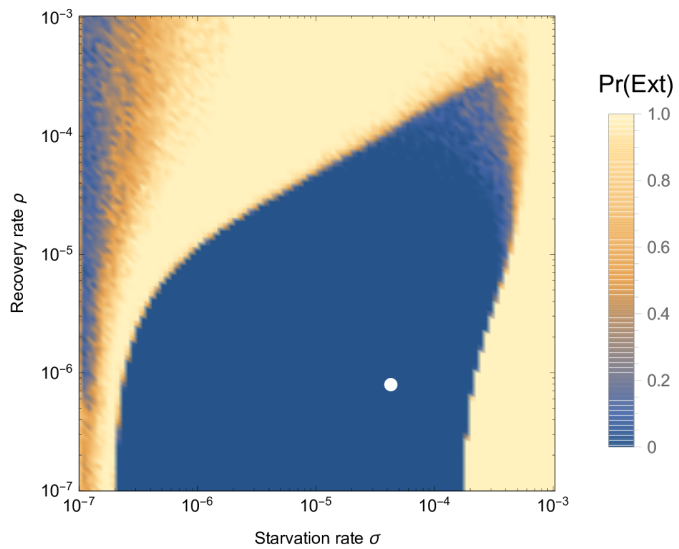


Fig. 5: Probability of extinction for a 100g consumer as a function of the starvation rate  $\sigma$  and recovery rate  $\rho$ , where the initial density is given as  $A(F^*, H^*, R^*)$ , with  $A$  being a random uniform variable in  $[0, 2]$ . Extinction is defined as the population trajectory falling below  $0.1 \times$  the allometrically constrained steady state. The white point denotes the allometrically constrained starvation and recovery rate.

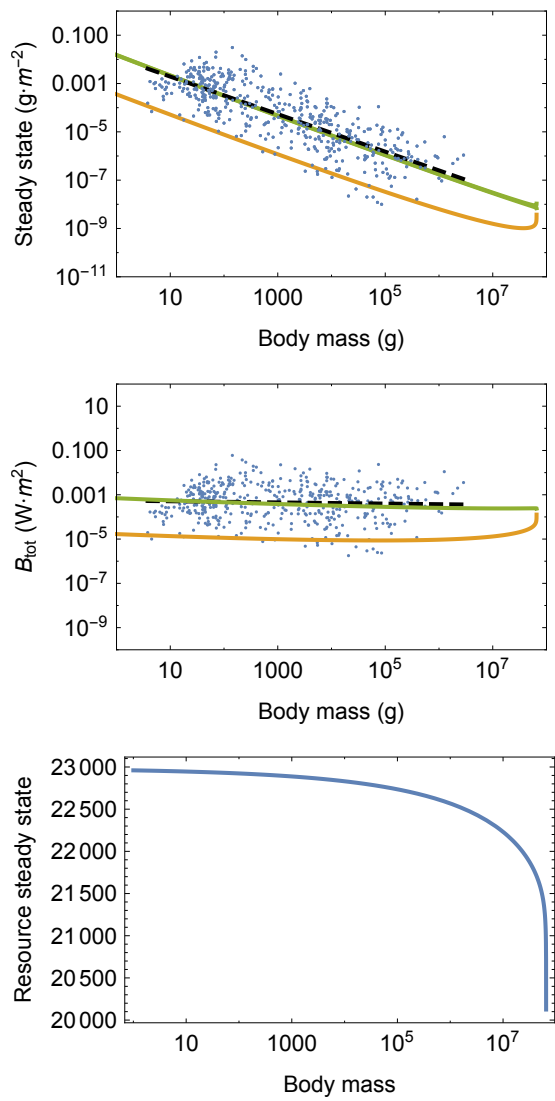


Fig. 6: (A) Consumer steady states  $F^*$  (green) and  $H^*$  (orange) as a function of body mass. (B) Total energetic use  $B_{\text{tot}}$  of consumer populations at the steady state as a function of body mass. (C) Resource steady state  $R^*$  as a function of consumer body mass.

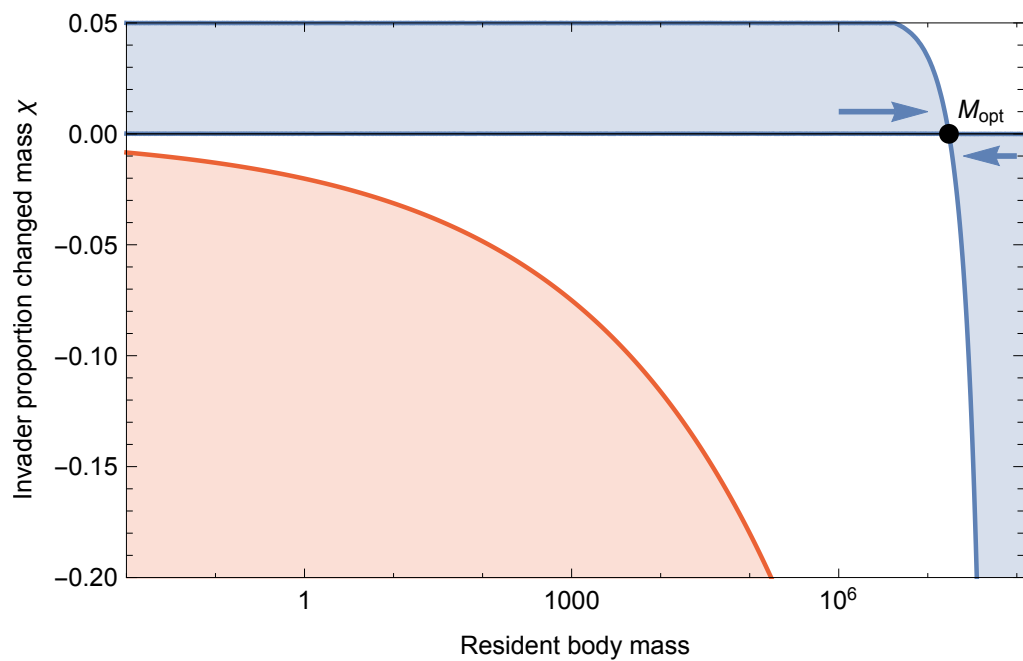


Fig. 7: Invasion feasibility for organisms with a proportional change in mass  $\chi$  against a population with a resident body mass  $M$ . The blue region denotes proportions of modified mass  $\chi$  resulting in successful invasion. The red region denotes values of  $\chi$  that result in a mass that is below the starvation threshold and is thus infeasible. Arrows point to the predicted optimal mass  $M_{\text{opt}} = 8.43 \times 10^6$ , which serves as the unininvadable, evolutionary stable state.